Journal of Scientific Computing, Vol. 16, No. 3, September 2001 (© 2001)

A Fat Boundary Method for the Poisson Problem in a Domain with Holes

Bertrand Maury[1]

Received November 10, 2000; accepted June 20, 2001

We consider the Poisson equation with Dirichlet boundary conditions, in a domain $\Omega \setminus \overline{B}$, where $\Omega \subset \mathbb{R}^n$, and B is a collection of smooth open subsets (typically balls). The objective is to split the initial problem into two parts: a problem set in the whole domain Ω, for which fast solvers can be used, and local subproblems set in narrow domains around the connected components of B, which can be solved in a fully parallel way. We shall present here a method based on a multi-domain formulation of the initial problem, which leads to a fixed point algorithm. The convergence of the algorithm is established, under some conditions on a relaxation parameter θ. The dependence of the convergence interval for θ upon the geometry is investigated. Some 2D computations based on a finite element discretization of both global and local problems are presented.

KEY WORDS: Finite element; Poisson equation; multiple-connected domains; fixed point algorithms; domain decomposition.

1. INTRODUCTION

Our purpose is to solve the Poisson equation in a domain $\Omega \setminus \overline{B}$, where $\Omega \subset \mathbb{R}^n$, and B is a collection of smooth subsets. We will consider the situation where Ω has a simple shape, so that the Poisson problem in Ω is "easy" to solve. Those problems arise in many modelling situations: thermal conductivity for composite materials, fluid flow in a porous, non-homogeneous medium, time-discretized fluid-particle flow problems. In the latter case, the "holes" are actually the moving particles, on which the velocity is known. For such problems, the domain in which the PDE is set can usually not be meshed in a structured way. Therefore standard fast

[1] Laboratoire d'Analyse Numérique, Université P. et M. Curie, 175 rue du Chevaleret, 75013 Paris, France. E-mail: maury@ann.jussieu.fr

0885-7474/01/0900-0319/0 © 2001 Plenum Publishing Corporation

solvers (based on a multilevel strategy, or FFT algorithms) cannot be used straightforwardly to compute the solution.

1.1. Existing Methods

We first present different strategies which have been carried out to solve numerically such problems. We shall consider here the homogeneous Dirichlet boundary conditions:

$$\begin{cases} -\triangle u = f & \text{in } \Omega \setminus B \\ u = 0 & \text{on } \partial\Omega \cup \partial B \end{cases} \tag{1}$$

1. Penalization. Let χ_B be the characteristic function of B, and $\varepsilon > 0$ a given (small) number. The initial problem 1 is replaced by

$$\begin{cases} \frac{1}{\varepsilon}\chi_B u - \triangle u = f & \text{in } \Omega \\ u = 0 & \text{on } \partial\Omega \end{cases} \tag{2}$$

   This method is easy to implement, but it is quite inaccurate near the boundary of B. Furthermore, the Laplace operator itself is highly modified, which prevents the use of standard fast solvers.

2. Boundary fitted mesh. The approximate solution is computed on a conforming, unstructured mesh, possibly refined in the neighbourhood of the holes. A detail of such an unstructured mesh is presented in Fig. 1.

   See [10] for an example of fluid-particle flow computations based on this approach. This method makes it possible to compute accurately in the neighbourhood of B, where usually high gradients of the solution can be expected, and less accurately far away

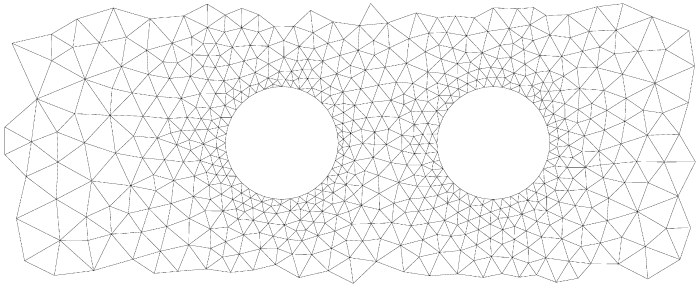

Fig. 1. Unstructured mesh.

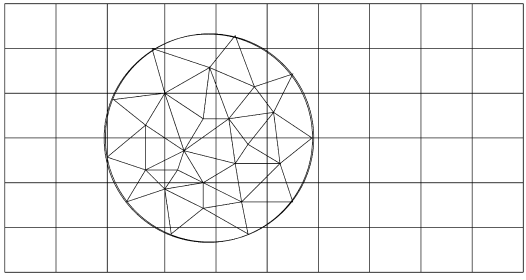

Fig. 2. Fictitious domain approach with distributed Lagrange Multipliers.

from B, where the solution is likely to be smooth. The main drawback is the loss of cartesian structure, which makes it difficult to find good preconditioners or to use fast solvers.

3. Fictitious domain method. The whole domain Ω is covered with a cartesian mesh, conforming meshes of the holes are built, and the boundary condition is taken into account by Lagrange multipliers which belong to a finite dimensional space associated to hole-meshes (see Fig. 2). This is the so-called fictitious domain approach with distributed Lagrange multipliers (see for example [3] or [4]). There exists also a version of this approach where the Lagrange multipliers are defined on the boundary of the hole (see [2]).

   Another version of the fictitious domain method is based on a locally fitted mesh (see Fig. 3). It gives a better approximation of the solution near the boundary. See [6] or [7] for an application of this method to the 3D Helmoltz equation.

4. Potential theory approach. This last class of methods relies on integral expressions of the solution rather than on direct discretization of the partial differential equation. Such methods have

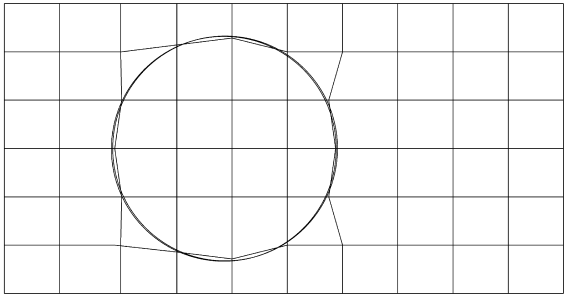

Fig. 3. Locally fitted mesh.

been made quite efficient in the recent years by combining the Fast Multipole Method for computing boundary integrals, and fast algorithms avoiding the use of any standard quadrature formula for computing volume integrals (see [5] and references therein).

1.2. Fat Boundary Method

Our purpose is to keep capability to compute accurately in the neighbourhood of the holes, but still to use a relative coarse cartesian mesh for computing the solution in the whole domain.

The method we propose is based on a splitting of the initial problem into local subproblems in the neighbourhood of B (in a crust-like zone around the holes, see Fig. 4, bottom) and global resolution on a cartesian mesh which covers the whole domain Ω. The link between global and local problems is based on

1. Interpolation of a globally defined field on an artificial boundary which delimits the local subdomain (like in the domain decomposition approach with full overlapping proposed by Letallec [8]).

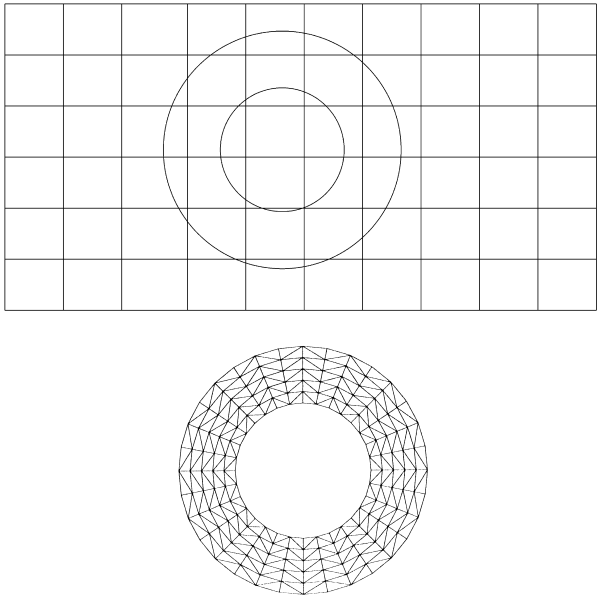

Fig. 4. Fat boundary: global and local meshes.

2. Prescription of a jump in normal derivative across the the boundary of B. This approach has been used in modelling immersed interfaces with finite differences on a cartesian mesh (see [9] or [11]). This singular source term in the Poisson equation will be handled here in the finite element framework.

The transition from the interpolated field to the normal derivative jump is based on Steklov–Poincaré-like operators associated to the narrow domains around the holes.

The paper is organized as follows. In Section 2 we introduce the multidomain formulation of the problem. In Section 3 we deduce a fixed point formulation, and show the convergence in the space-continuous case of a relaxed algorithm, under some conditions on the relaxation parameter. In Section 4 we give some results on the behaviour of the constants involved in the sufficient condition of convergence. Finally, in Section 5, we present two examples of finite element computations.

2. NOTATIONS: MULTIDOMAIN FORMULATION

We consider a Lipschitz bounded domain $\Omega \subset \mathbb{R}^n$ and $B \subset \Omega$ a smooth subdomain. Figure 5 represents the case of a single hole in the domain, but the analysis is still valid in the case of a multi-connected domain B. In the latter situation, we will simply assume that the "crust-like" domains around the connected component of B do not overlap. The boundaries of Ω and B are denoted by Γ and γ, respectively. We shall use the functional spaces

$$H_0^1(\Omega) = \{\hat{u} \in H^1(\Omega),\ \hat{u}_{|\Gamma} = 0\} \tag{3}$$

$$H_0^1(\Omega \setminus \bar{B}) = \{u \in H^1(\Omega \setminus \bar{B}),\ u_{|\Gamma} = 0\} \tag{4}$$

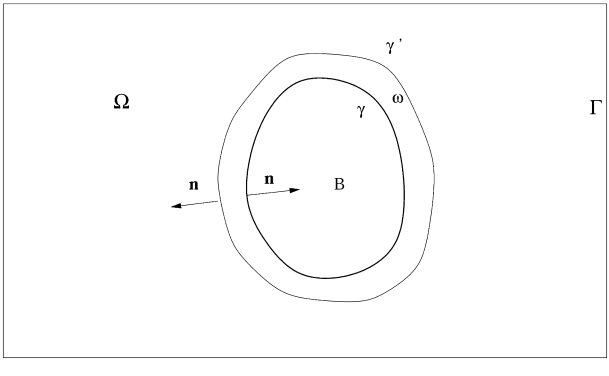

Fig. 5. Domains in the case $n = 2$.

(note that functions in $H_0^1(\Omega \setminus \bar{B})$ do not necessarily vanish on γ). Let $f \in L^2(\Omega \setminus \bar{B})$. Our purpose is to solve the problem I: Find $u \in H_0^1(\Omega \setminus \bar{B})$, such that

$$\text{I} \begin{cases} -\triangle u = f & \text{in } \Omega \setminus \bar{B} \\ u_{|\gamma} = 0 \end{cases} \tag{5}$$

We consider a proper superset of B, $B^* \supset B$, completely contained in Ω, and we take $\omega = B^* \setminus \bar{B}$. The boundary of ω is $\partial\omega = \gamma \cup \gamma'$ (see Fig. 5). We introduce the new functional space

$$H_0^1(\omega) = \{v \in H^1(\omega),\ v_{|\gamma} = 0\} \tag{6}$$

The spaces $H_0^1(\Omega)$, $H_0^1(\Omega \setminus \bar{B})$, $H_0^1(\omega)$ are endowed with the Hilbert norms

$$|\hat{u}|^2_{H_0^1(\Omega)} = \int_\Omega |\nabla \hat{u}|^2, \qquad |u|^2_{H_0^1(\Omega \setminus \bar{B})} = \int_{\Omega \setminus \bar{B}} |\nabla u|^2, \qquad |v|^2_{H_0^1(\omega)} = \int_\omega |\nabla v|^2 \tag{7}$$

For a function f defined in $\Omega \setminus \bar{B}$, we denote by $\bar{f}$ its extension by 0 in B:

$$\bar{f}_{|\Omega \setminus \bar{B}} = f_{|\Omega \setminus \bar{B}}, \qquad \bar{f}_{|B} = 0 \tag{8}$$

The extension operator for functions defined in ω is defined in a similar manner. Our purpose is to replace problem I by a couple of new ones, one of which is set in ω, and the other one in the whole domain Ω: Find $(\hat{u}, v) \in H_0^1(\Omega) \times H_0^1(\omega)$ such that

$$\text{II} \begin{cases} \text{a: } \begin{cases} -\triangle v = f & \text{in } \omega \\ v_{|\gamma'} = \hat{u}_{|\gamma'} \end{cases} \\ \text{b: } -\triangle \hat{u} = \bar{f} + \left.\dfrac{\partial v}{\partial n}\right|_\gamma \delta_\gamma \qquad \text{in } \Omega \end{cases} \tag{9}$$

In the previous equation, $\frac{\partial v}{\partial n}|_\gamma\, \delta_\gamma \in H^{-1}(\Omega)$ stands for the linear form

$$\hat{u} \in H_0^1(\Omega) \longmapsto \int_\gamma \frac{\partial v}{\partial n} \hat{u} \tag{10}$$

which is continuous since v belongs to $H_0^1(\omega)$ and $\triangle v$ to $L^2(\omega)$. Let us first establish the link between the two problems:

Proposition 2.1. Problems I and II are equivalent, i.e.,

(i) If $u \in H_0^1(\Omega \setminus \bar{B})$ is a solution of problem I, then the couple $(\bar{u}, u_{|\omega})$ is a solution of problem II.

(ii) If $(\hat{u}, v)$ is a solution of problem II, then $\hat{u}_{|\Omega \setminus \bar{B}}$ is a solution of problem I.

Proof. (i) Let $u \in H_0^1(\Omega \setminus \bar{B})$ be a solution of I. Then the function $v = u_{|\omega}$ is clearly a solution of II.a (as $\bar{u}_{|\gamma'} = u_{|\gamma'}$). The extension of u by 0, $\bar{u}$, verifies

$$\begin{aligned} -\triangle \bar{u} &= \bar{f} \qquad \text{in } \Omega \setminus \bar{B} \\ -\triangle \bar{u} &= \bar{f} \qquad \text{in } B \end{aligned} \tag{11}$$

For any test function $w \in H_0^1(\Omega)$, we multiply those equations by $w_{|\Omega \setminus \bar{B}}$ and $w_{|B}$, respectively, integrate by parts, and sum up the obtained equations:

$$\int_\Omega \nabla \bar{u} \cdot \nabla w + \int_\gamma \frac{\partial \bar{u}}{\partial n}\bigg|_i w - \int_\gamma \frac{\partial \bar{u}}{\partial n}\bigg|_e w = \int_\Omega \bar{f} w \tag{12}$$

(the letters i and e stand for interior and exterior, respectively) with $\partial \bar{u}/\partial n|_i = 0$ and $\partial \bar{u}/\partial n|_e = \partial u/\partial n$, so that

$$\int_\Omega \nabla \bar{u} \cdot \nabla w = \int_\Omega \bar{f} w + \int_\gamma \frac{\partial u}{\partial n} w \tag{13}$$

which leads (by backward integration of the integral over Ω) to II.b:

$$-\triangle \bar{u} = \bar{f} + \frac{\partial u}{\partial n}\delta_\gamma = \bar{f} + \frac{\partial v}{\partial n}\delta_\gamma \tag{14}$$

(ii) Let $(\hat{u}, v) \in H_0^1(\Omega) \times H_0^1(\omega)$ be a solution of problem II. The very same approach as (i) ensures that $\bar{v} = \hat{u}_{|\bar{B} \cup \omega}$, so that $\hat{u} \equiv 0$ in B, and consequently $\hat{u}_{|\gamma} = 0$. Therefore $\hat{u}_{|\Omega \setminus \bar{B}}$ is a solution of problem I. □

2.1. Non-Homogeneous Boundary Conditions

The previous formulation can be extended to the case of non-homogeneous boundary conditions on γ (the case of non-homogeneous boundary conditions on Γ is standard)

$$\begin{cases} -\triangle u = f & \text{in } \Omega \setminus B \\ u = 0 & \text{on } \Gamma \\ u = g & \text{on } \gamma \end{cases} \tag{15}$$

with $g \in H^{1/2}(\gamma)$. Let w be a harmonic extension of g in B. We have equivalence between (15) and the multidomain formulation

$$\text{II} \begin{cases} \text{a:} \begin{cases} -\triangle v = f & \text{in } \omega \\ v|_{\gamma'} = \hat{u}_{|\gamma'} \\ v_{|\gamma} = g \end{cases} \\ \text{b:} -\triangle \hat{u} = \bar{f} + \left(\dfrac{\partial v}{\partial n} - \dfrac{\partial w}{\partial n} \right)\Big|_{\gamma} \delta_{\gamma} \qquad \text{in } \Omega \end{cases} \tag{16}$$

where the normal derivative of w is taken inward with respect to B.

Remark 2.1. Another formulation, which can be useful when the harmonic extension cannot be calculated analytically, consists in taking for w any extension of g in B. We assume g to be $H^{3/2}(\gamma)$. Hence we can take $w \in H^2(B)$, so that $\triangle w$ is in $L^2(B)$, and its extension by 0 in $\Omega \setminus \bar{B}$ is well defined as an element of $L^2(\Omega)$. The problem II.b is then written

$$-\triangle \hat{u} = \bar{f} + \left(\frac{\partial v}{\partial n} - \frac{\partial w}{\partial n} \right)\Big|_{\gamma} \delta_{\gamma} - \triangle w \qquad \text{in } \Omega \tag{17}$$

3. SOLUTION METHOD

3.1. Fixed Point Formulation

Our aim is to transform problem II into a fixed point problem. Let θ be a real parameter in $]0, 1[$ (relaxation parameter). The operator we will consider is

$$\mathbf{T}_{\theta} : (\hat{u}, v) \in H_0^1(\Omega) \times H_0^1(\omega) \longmapsto (\hat{U}, V) \tag{18}$$

where $V \in H_0^1(\omega)$ and $\hat{U} \in H_0^1(\Omega)$ are solutions of

$$\begin{cases} -\triangle V = f & \text{in } \omega \\ V_{|\gamma'} = (\theta v + (1-\theta)\hat{u})_{|\gamma'} \end{cases} \tag{19}$$

and

$$-\triangle \hat{U} = \bar{f} + \frac{\partial V}{\partial n} \delta_{\gamma} \qquad \text{in } \Omega \tag{20}$$

respectively. By definition of $\mathbf{T}_\theta$, we have immediately the fixed point formulation, which holds for any $\theta \neq 1$,

$$(\hat{u}, v) \text{ is a solution of II} \Leftrightarrow \mathbf{T}_\theta(\hat{u}, v) = (\hat{u}, v) \tag{21}$$

3.2. Iterative Algorithm

Our purpose is now to prove the convergence of sequences in $H_0^1(\Omega) \times H_0^1(\omega)$ obtained by successive iterations of $\mathbf{T}_\theta$:

$$(\hat{u}^{m+1}, v^{m+1}) = \mathbf{T}_\theta(\hat{u}^m, v^m) \tag{22}$$

to the exact solution of problem II, possibly under some restrictions on θ. We will consider only the case $f \equiv 0$. Indeed, if $(\hat{u}_0, v_0)$ is the fixed point of $\mathbf{T}_\theta$, then by translating the sequence

$$(\hat{u}^m, v^m) \longmapsto (\hat{u}^m - \hat{u}_0, v^m - v_0) \tag{23}$$

we recover the homogeneous case.

We introduce the linear operators **D** and **N**:

$$\mathbf{D}: H_0^1(\Omega) \longrightarrow H_0^1(\omega) \tag{24}$$

$$\hat{u} \longmapsto \mathbf{D}\hat{u} = V, \text{ solution of II.a: } \begin{cases} -\triangle V = 0 & \text{in } \omega \\ V_{|\gamma'} = \hat{u}_{|\gamma'} \end{cases} \tag{25}$$

and

$$\mathbf{N}: H_0^1(\omega) \longrightarrow H_0^1(\Omega) \tag{26}$$

$$v \longmapsto \mathbf{N}v = \hat{U}, \text{ solution of II.b: } -\triangle \hat{U} = \left.\frac{\partial v}{\partial n}\right|_\gamma \delta_\gamma \qquad \text{in } \Omega \tag{27}$$

In order to establish the main result, we will need the following lemma, related to the restriction of **ND** to $R(\mathbf{N})$, the range of **N**:

Lemma 3.1. The operator $\mathbf{ND}: H_0^1(\Omega) \longrightarrow H_0^1(\Omega)$ is continuous:

$$\exists C > 0, \qquad |\mathbf{ND}\hat{u}| \leqslant C\,|\hat{u}| \tag{28}$$

and verifies

$$(\mathbf{ND}\hat{u}, \hat{u}) \leqslant 0 \qquad \forall \hat{u} \in R(\mathbf{N}) \tag{29}$$

Proof. We introduce $V = \mathbf{D}\hat{u}$ and $\hat{U} = \mathbf{ND}\hat{u} = \mathbf{N}V$. The continuity of **ND** comes from the continuity of operators:

$$\begin{array}{c} \hat{u} \in H_0^1(\Omega) \longmapsto \quad \hat{u}_{|\gamma'} \in H^{1/2}(\gamma') \\ \downarrow \\ V \in H_0^1(\omega) \\ \downarrow \\ \left.\dfrac{\partial V}{\partial n}\right|_{\gamma} \in H^{-1/2}(\gamma) \longmapsto \hat{U} \in H_0^1(\Omega) \end{array} \tag{30}$$

so that

$$\exists C > 0, \qquad |\hat{U}| \leqslant C\,|\hat{u}| \tag{31}$$

Let us now prove that $(\mathbf{ND}\hat{u}, \hat{u}) \leqslant 0$, i.e., $(\hat{U}, \hat{u}) \leqslant 0$. Firstly, we use the fact that $\hat{U} = \mathbf{N}V$, and we take $\hat{u}$ as a test function:

$$(\mathbf{ND}\hat{u}, \hat{u}) = \int_{\Omega} \nabla\hat{U} \cdot \nabla\hat{u} = \int_{\gamma} \frac{\partial V}{\partial n}\,\hat{u} \tag{32}$$

As $\hat{u} \in R(\mathbf{N})$, it is solution of

$$-\triangle\hat{u} = g\delta_{\gamma} \tag{33}$$

for a certain $g \in H^{-1/2}(\gamma)$. We multiply (33) by V, and integrate over ω using the fact that $V_{|\gamma} = 0$:

$$\int_{\omega} \nabla\hat{u} \cdot \nabla V - \int_{\gamma'} \frac{\partial\hat{u}}{\partial n} V = 0 \tag{34}$$

Integrating again by parts, it comes

$$-\int_{\omega} \hat{u}\triangle V + \int_{\gamma} \frac{\partial V}{\partial n}\,\hat{u} + \int_{\gamma'} \frac{\partial V}{\partial n}\,\hat{u} - \int_{\gamma'} \frac{\partial\hat{u}}{\partial n} V = 0 \tag{35}$$

so that

$$\int_{\gamma} \frac{\partial V}{\partial n}\,\hat{u} = \int_{\gamma'} \frac{\partial\hat{u}}{\partial n} V - \int_{\gamma'} \frac{\partial V}{\partial n}\,\hat{u} \tag{36}$$

which implies ($V_{|\gamma'} = \hat{u}_{|\gamma'}$)

$$(\mathbf{ND}\hat{u}, \hat{u}) = \int_\gamma \frac{\partial V}{\partial n}\hat{u} = \int_{\gamma'} \frac{\partial \hat{u}}{\partial n}\hat{u} - \int_{\gamma'} \frac{\partial V}{\partial n} V \tag{37}$$

We now remark that

$$\begin{cases} -\triangle \hat{u} = 0 & \text{in } \Omega \setminus (\bar{B} \cup \omega) \\ \hat{u}_{|\Gamma} = 0 \end{cases} \tag{38}$$

which implies (with the normal derivative taken outward relatively to ω, as in (37))

$$\int_{\gamma'} \frac{\partial \hat{u}}{\partial n}\hat{u} = -\int_{\Omega \setminus (\bar{B} \cup \bar{\omega})} |\nabla \hat{u}|^2 \leqslant 0 \tag{39}$$

Similarly,

$$\begin{cases} -\triangle V = 0 & \text{in } \omega \\ V_{|\gamma} = 0 \end{cases} \tag{40}$$

implies

$$\int_{\gamma'} \frac{\partial V}{\partial n} V = \int_\omega |\nabla V|^2 \geqslant 0 \tag{41}$$

Finally, equation (37) and inequalities (39) and (41) yield

$$\int_\gamma \frac{\partial V}{\partial n}\hat{u} \leqslant 0 \tag{42}$$

therefore $\int_\Omega \nabla \hat{U} \cdot \nabla \hat{u} \leqslant 0$. □

We may now establish the main property, which will ensure the conditional convergence of the algorithm. The constant C denotes any upper bound of $\|\mathbf{ND}\|_{\mathscr{L}(H^1_0(\Omega))}$ (see Eq. (28)).

Proposition 3.1. For any $\theta \in]1-2/(1+C)^2, 1[$, there exist constants $k \in]0, 1[$ and $C_{\mathbf{D}} > 0$ such that, for any $(\hat{u}, v) \in R(\mathbf{T}_\theta)$,

$$|\hat{U}| \leqslant k\,|\hat{u}| \tag{43}$$

and

$$|V| \leqslant \theta\,|v| + C_{\mathbf{D}}\,|\hat{u}| \tag{44}$$

where $(\hat{U}, V) = \mathbf{T}_\theta(\hat{u}, v)$. The optimal k is obtained for $\theta = \theta_{\text{opt}} = 1 - 1/(1+C)^2$, and its value is $k_{\text{opt}} = \sqrt{\theta_{\text{opt}}}$.

Proof. As $V = \theta v + (1-\theta)\,\mathbf{D}\hat{u}$, inequality (44) is a direct consequence of the continuity of $\mathbf{D}$: $H_0^1(\Omega) \longrightarrow H_0^1(\omega)$:

$$|\mathbf{D}\hat{u}| \leqslant C_{\mathbf{D}}\,|\hat{u}| \tag{45}$$

Let us now prove the existence of $k \in]0, 1[$ such that (43) is satisfied. As $(\hat{u}, v)$ is in $R(\mathbf{T}_\theta)$, $\hat{u} = \mathbf{N}v$, so that

$$\hat{U} = \mathbf{N}V \tag{46}$$

$$= \theta\mathbf{N}v + (1-\theta)\,\mathbf{ND}\hat{u} \tag{47}$$

$$= \theta\hat{u} + (1-\theta)\,\mathbf{ND}\hat{u} \tag{48}$$

$$= \hat{u} - (1-\theta)(\hat{u} - \mathbf{ND}\hat{u}) \tag{49}$$

We have

$$|\hat{U}|^2 = |\hat{u}|^2 - 2(1-\theta)(\hat{u} - \mathbf{ND}\hat{u}, \hat{u}) + (1-\theta)^2\,|\hat{u} - \mathbf{ND}\hat{u}|^2 \tag{50}$$

Using Lemma 3.1, it comes

$$|\hat{U}|^2 \leqslant |\hat{u}|^2\,(1 - 2(1-\theta) + (1+C)^2\,(1-\theta)^2) \tag{51}$$

Then, for any $\theta \in]1 - \frac{2}{(1+C)^2}, 1[$,

$$k = \sqrt{1 - 2(1-\theta) + (1+C)^2(1-\theta)^2} < 1 \tag{52}$$

which proves (43). The optimal k is simply obtained by minimization of (52), which gives $1-\theta = 1/(1+C)^2$ and consequently $k = (1 - 1/(1+C)^2)^{1/2}$. □

Remark 3.1. As we need inequality (45) only for $\hat{u} \in R(\mathbf{N})$, we can define $C_{\mathbf{D}}$ as the norm of $\mathbf{D}$ restricted to functions which are harmonic in B and in $\Omega \setminus \bar{B}$. Similarly, we define $C_{\mathbf{N}}$ as the norm of $\mathbf{N}$ restricted to functions which are harmonic in ω. The constant C which determines the convergence interval can be taken equal to the product $C_{\mathbf{N}}C_{\mathbf{D}}$. Note that it is in general strictly less than the norm of $\mathbf{ND} \in \mathscr{L}(H_0^1(\Omega))$.

As a direct consequence of Proposition 3.1, we have the

Corollary 3.1. We assume that $\theta \in]1-2/(1+C)^2, 1[$. Then for any

$$(\hat{u}^0, v^0) \in H_0^1(\Omega) \times H_0^1(\omega) \tag{53}$$

the sequence $(\hat{u}^m, v^m)$ defined by

$$(\hat{u}^{m+1}, v^{m+1}) = \mathbf{T}_\theta(\hat{u}^m, v^m) \tag{54}$$

converges to (0, 0).

Proof. Let the sequence $(\alpha^m, \beta^m)_{n \geqslant 1} \in \mathbb{R}^2$ be defined by

$$\begin{pmatrix} \alpha^1 \\ \beta^1 \end{pmatrix} = \begin{pmatrix} |\hat{u}^1| \\ |v^1| \end{pmatrix} \tag{55}$$

$$\begin{pmatrix} \alpha^{m+1} \\ \beta^{m+1} \end{pmatrix} = \begin{pmatrix} k & 0 \\ C_{\mathrm{D}} & \theta \end{pmatrix} \begin{pmatrix} \alpha^m \\ \beta^m \end{pmatrix} = A \begin{pmatrix} \alpha^m \\ \beta^m \end{pmatrix} \tag{56}$$

As $(\hat{u}^m, v^m)$ is in $R(\mathbf{T}_\theta)$ as soon as $m \geqslant 1$, it is clear from (43) and (44) that $|\hat{u}^m| \leqslant \alpha^m$ and $|v^m| \leqslant \beta^m$, for all $m \geqslant 1$. As the spectral radius $\rho(A) = \max(k, \theta)$ is strictly less than 1, the sequence (α^m, β^m) converges to (0, 0), and so does $(|\hat{u}^m|, |v^m|)$. □

4. CONSTANT ESTIMATION

In this section, we investigate the dependence of C upon geometrical parameters. In order to get an explicit expression of C, we shall restrict ourselves to a simplified situation: Γ, γ, and γ' are concentric spheres of $\mathbb{R}^n$, and all functions are radial. It corresponds to the case in which the data $f \in L^2(\Omega \setminus \bar{B})$ is itself radial.

We denote by r the radius of γ, by ε the width of ω (so that $r+\varepsilon$ is the radius of γ'), and by L the distance between Γ and γ, so that the radius of Γ is $r+L$. We introduce the system of polar coordinates (ρ, σ) with respect to the common center of the spheres. Following [1, p. 530], we denote by Σ the unit sphere of $\mathbb{R}^n$, and by σ a point on it. The polar definition of ω and Ω is

$$\omega_{\rho,\sigma} =]r, r+\varepsilon[\times \Sigma, \qquad \Omega_{\rho,\sigma} =]r, r+L[\times \Sigma \tag{57}$$

Proposition 4.1. Let $r > 0$ be given. We consider the situation

$$L \longrightarrow +\infty, \qquad \varepsilon \longrightarrow 0 \tag{58}$$

The behaviour of constant C is

$$\begin{cases} C \sim \dfrac{L}{\varepsilon} & \text{in the case} \quad n=1 \\ C \sim \dfrac{r}{\varepsilon} \ln L & \text{in the case} \quad n=2 \\ C \sim \dfrac{r}{\varepsilon} & \text{in the case} \quad n=3 \end{cases} \tag{59}$$

Proof. Following Remark 3.1, we shall consider only harmonic functions to estimate C. Note that in this simplified framework, $H_0^1(\omega)$ and $H_0^1(\Omega)$ are monodimensional.

Case $n=1$. All harmonic functions are affine, so that C_{D} and C_{N} can be explicitly found.

Case $n=2$. A radial function of $H_0^1(\Omega)$, piecewise harmonic with respect to B and $\Omega \setminus \bar{B}$, can be expressed $w(\rho, \sigma) = w(\rho) = \alpha \ln(\rho/(r+L))$ for $\rho > r$, and $w(\rho, \sigma) = \alpha \ln(r/(r+L))$ for $\rho \leqslant B$, so that $\|D\|$ is given by

$$\|D\|^2 = \frac{\int_\omega |\nabla v|^2}{\int_{\Omega \setminus \bar{B}} |\nabla \hat{u}|^2} = \frac{|\Sigma| \int_{]r,\, r+\varepsilon[} |\partial_r v|^2 \, \rho \, d\rho}{|\Sigma| \int_{]r,\, r+L[} |\partial_r \hat{u}|^2 \, \rho \, d\rho} \tag{60}$$

where

$$\hat{u} = \ln\left(\frac{\rho}{r+L}\right), \qquad v = v(\rho, \sigma) = \frac{\ln\left(\dfrac{r+\varepsilon}{r+L}\right)}{\ln\left(\dfrac{r+\varepsilon}{r}\right)} \ln(\rho/r) \tag{61}$$

It gives

$$C_{\mathrm{D}} \sim \left(\frac{r}{\varepsilon} \ln L\right)^{1/2} \tag{62}$$

To compute C_{N} we perform the same approach with

$$v(\rho, \sigma) = v(\rho) = \ln\left(\frac{\rho}{r}\right), \qquad \hat{u} = \mathbf{N}v = \ln\left(\frac{\rho}{L}\right) \tag{63}$$

which gives

$$C_{\mathrm{N}} = \left(\frac{\ln(1+\varepsilon/r)}{\ln(1+L/r)}\right)^{1/2} \sim \left(\frac{r}{\varepsilon} \ln L\right)^{1/2} \tag{64}$$

We finally get $C = C_{\mathrm{N}} C_{\mathrm{D}} \sim \frac{r}{\varepsilon} \ln L$.

Case $n=3$. A radial function of $H_0^1(\Omega)$, piecewise harmonic with respect to B and $\Omega \setminus \bar{B}$, can be expressed $w(\rho, \sigma) = w(\rho) = \alpha(1-(r+L)/\rho)$ for $\rho > r$, $w(\rho, \sigma) = -\alpha L/r$ for $\rho \leqslant r$. Straightforward calculations similar to the case $n = 2$ give

$$C_{\mathrm{D}} \sim \left(\frac{r}{\varepsilon}\right)^{1/2}, \qquad C_{\mathrm{N}} \sim \left(\frac{r}{\varepsilon}\right)^{1/2} \tag{65}$$

which leads to the third estimate. □

Remark 4.1. It is well-known that there is no non-zero radial harmonic function in the unbounded domain $\mathbb{R}^n \setminus \bar{B}$, decreasing to 0 when $|\mathbf{x}|$ grows to $+\infty$, unless $n \geqslant 3$. This property appears in the dependence upon L of C in the cases $n = 1$ and $n = 2$.

Remark 4.2. The estimation of C_{D} in the radial case is closely related to the notion of capacity of a compact set on a domain (see [1, p. 433]). Indeed, if we denote by $\mathrm{cap}_{\mathcal{O}}(K)$ the capacity on a domain $\mathcal{O}$ of a compact $K \subset \mathcal{O}$, one can check that

$$C_{\mathrm{D}} \sim \left(\frac{\mathrm{cap}_{\Omega \setminus \bar{B}}(\Omega \setminus (\bar{B} \cup \omega))}{\mathrm{cap}_{\Omega}(B)}\right)^{1/2} \tag{66}$$

5. NUMERICAL EXPERIMENTS

5.1. Space Discretization. Algorithm

We introduce P^1 finite element approximation spaces

$$X_h^{\Omega} \subset H_0^1(\Omega), \qquad X_h^{\omega} \subset H_0^1(\omega) \tag{67}$$

The space X_h^{Ω} is based on a structured mesh of $\Omega = [0, 1] \times [0, 1]$, and X_h^{ω} corresponds to a mesh similar to the one represented in Fig. 4. A step of the algorithm is:

1. Compute $\hat{u}_h^{k-1}|_{\gamma_h'}$, the interpolation of $\hat{u}_h^{k-1}$ on γ_h', and set

$$\alpha_h^k = \theta \alpha_h^{k-1} + (1-\theta)\, \hat{u}_h^{k-1}|_{\gamma_h'} \tag{68}$$

The field α_h^k is defined pointwise at the vertices of γ_h'. It is identified with the corresponding piecewise P^1 function on γ_h'.

2. Compute $v_h^k \in X_h^\omega$, the solution of

$$\begin{cases} \int_\omega \nabla v_h^k \cdot \nabla w = \int_\omega f w \qquad \forall w \in X_h^\omega \quad w|_{\gamma_h'} = 0 \\ v_h^k|_{\gamma'} = \alpha_h^k \end{cases} \tag{69}$$

3. Compute

$$\varphi_h^k = \left.\frac{\partial v_h^k}{\partial n}\right|_{\gamma^h} \tag{70}$$

Note that, as a trace of the gradient of a piecewise P^1 function, φ_h^k is piecewise constant on γ_h.

4. Compute $\hat{u}_h^k \in X_h^\Omega$, the solution of

$$\int_\Omega \nabla \hat{u}_h^k \cdot \nabla w = \int_\omega \bar{f} w + \int_{\gamma_h} \varphi_h^k w \qquad \forall w \in X_h^\Omega \tag{71}$$

5.2. Computational Aspects

5.2.1. Matrices

The matrices associated to local and global problems are assembled, and Cholesky factorizations are performed before the fixed point loop. Note that in the case of identical holes, a single matrix has to be assembled and factorized for all the local problems.

5.2.2. Boundary Integral

The boundary integral in the right-hand side of Eq. (71) is computed by a simple quadrature formula. For any test function w, any segment S of γ_h, we use

$$\int_{\gamma_h} \varphi_h^k \approx \varphi_h^k|_S \; w(\mathbf{x}_S) \; |S| \tag{72}$$

where $\mathbf{x}_S$ is the center of S, and $|S|$ its length.

5.3. Test Cases

5.3.1. Many-Holes Computation

The first example illustrate the capability to deal with complex geometries. It corresponds to the situation represented in Fig. 6. The number of

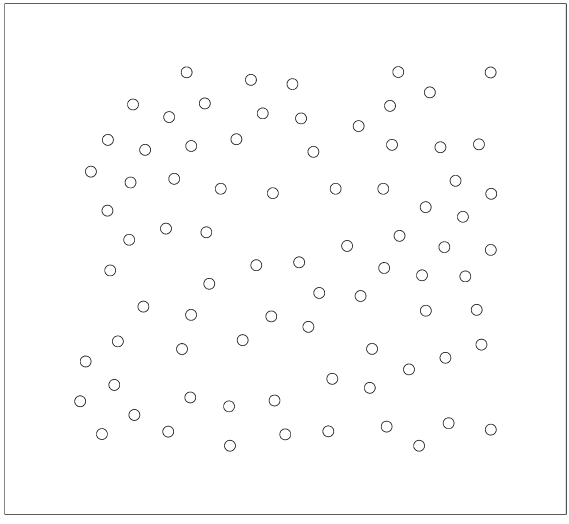

Fig. 6. Geometry of the problem: Γ and γ.

holes is 80 and their common radius is 0.01. The value of the relaxation parameter θ is 0.97. We used a 160×160 cartesian mesh for Ω, and local 40×40 meshes around the holes. All those meshes are the identical up to a translation. Note that the diameter of the holes is only 3 times the global mesh step size. The problem we solve is

$$\begin{cases} -\triangle u = 1 & \text{in } \Omega \setminus \bar{B} \\ u = 0 & \text{on } \Gamma \cup \gamma \end{cases} \tag{73}$$

Figure 7 represents the contours of the approximate solution.

5.3.2. Nonconstant Boundary Conditions

The second example shows how the use of a local fine mesh make it possible to capture a local oscilating behaviour of the solution. We introduce the polar coordinate system $(\rho, \sigma) \in \mathbb{R}^+ \times [0, 2\pi[$ centered at (0.5, 0.5). The domain B is the disk $\{\rho \leqslant r\}$, and γ' is the circle $\{\rho = r + \varepsilon\}$. The problem we solve is

$$\begin{cases} -\triangle u = 0 & \text{in } \Omega \setminus \bar{B} \\ u = g = \sin(m\sigma) & \text{on } \gamma \\ u = \left(\dfrac{\rho}{r}\right)^m \sin(m\sigma) & \text{on } \Gamma \end{cases} \tag{74}$$

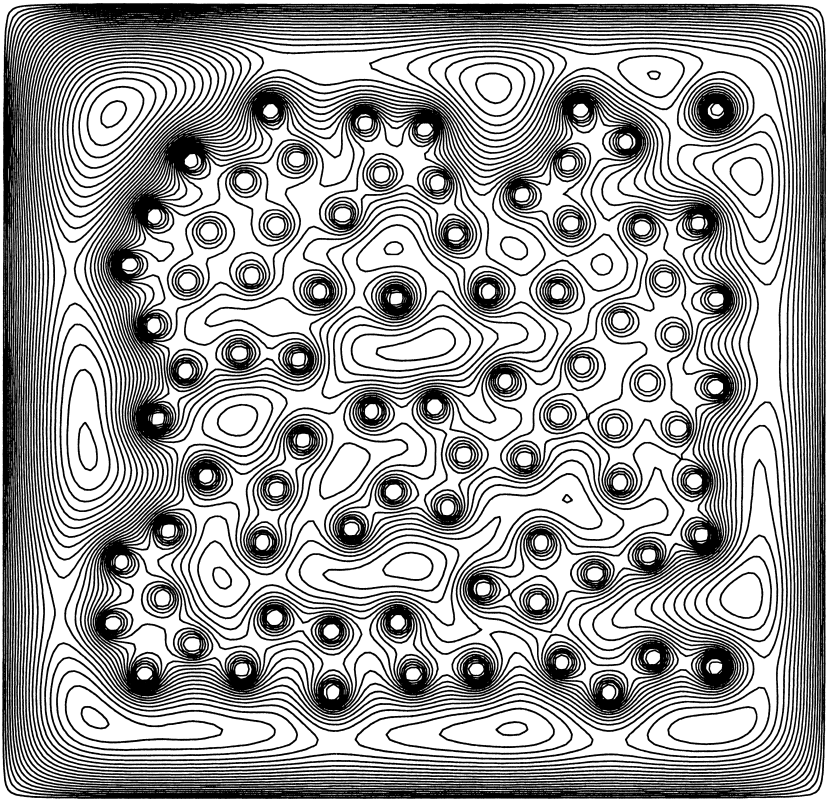

Fig. 7. Contours of the approximate solution.

for which $u_e = (\rho/r)^m \sin(m\sigma)$ is an exact solution. The numerical values are

$$m = -8, \qquad r = 0.15, \qquad \varepsilon = 0.03, \qquad \theta = 0.8 \tag{75}$$

As described in Section 2.1, we need an extension u_g of g in B. In the present case, we have the analytic expression of a harmonic extension: $u_g = (\rho/r)^{|m|} \sin(m\sigma)$, with

$$\left.\frac{\partial u_g}{\partial n}\right|_\gamma = \frac{|m|}{\rho}\left(\frac{\rho}{r}\right)^{|m|-1} \sin(m\sigma)|_{\rho=r} = \frac{|m|}{r}\sin(m\sigma) \tag{76}$$

Figures 8 and 9 represent the computed solution on Ω and ω, respectively. For the sake of clarity, we used a cartesian representation of the polar

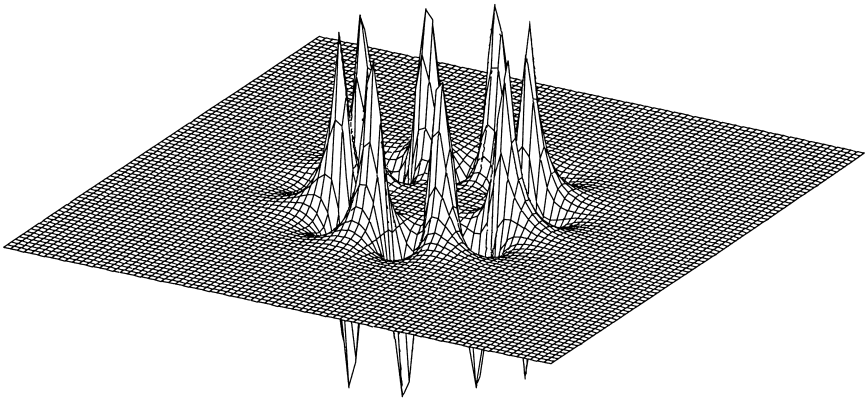

Fig. 8. Approximate solution in Ω.

coordinate system in ω. We used $n \times n$ meshes for both Ω and ω (so that the global mesh is much coarser than the local one). Several computations were performed, for different values of n ($n = 80$ in Figs. 10 and 11). Figure 10 shows the dependence of the local error

$$e = \left(\int_{\omega} |\nabla v_h - \nabla v_e|^2 \, d\omega \right)^{1/2} \tag{77}$$

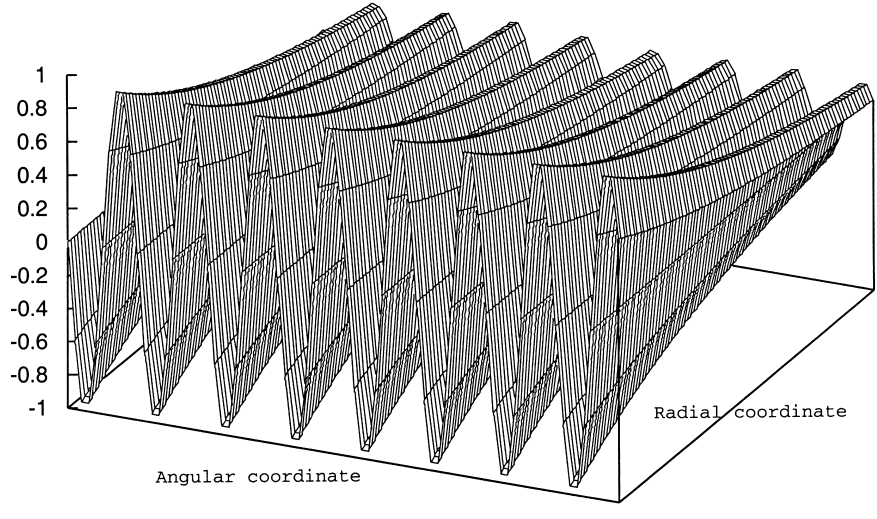

Fig. 9. Approximate solution in ω.

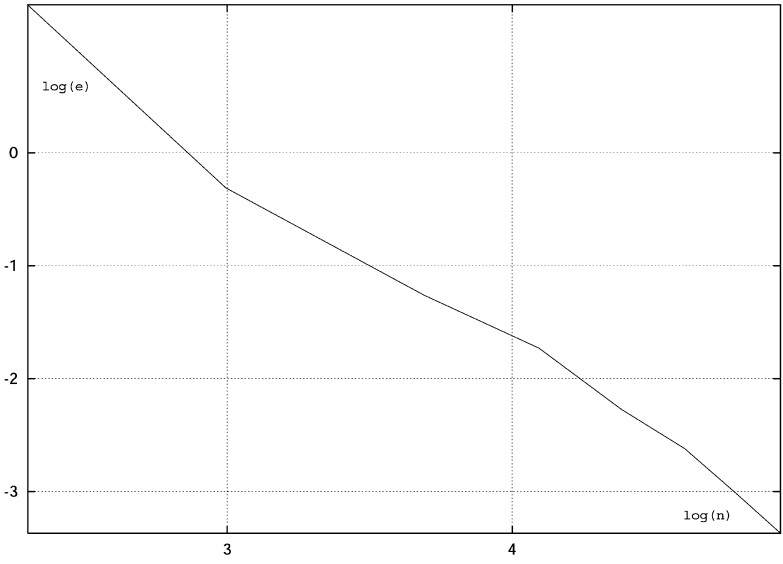

Fig. 10. H^1 error vs. $1/h$ in log–log scale.

upon the mesh step size $h = 1/n$. The field v_h is the solution obtained after 20 iterations of the fixed point algorithm, and v_e is the restriction of the exact solution to ω. The log–log plot indicates a first order convergence of error e to 0, when both mesh step sizes decrease together to 0.

6. CONCLUSION

We proposed a new method to solve elliptic problems in domains with holes. Its main features are

- The computation on the whole domain is based on a cartesian mesh, and the discretized operator does not depend on the geometry (positions and sizes of the holes). It makes it possible to use fast, easily parallelizable solvers for this part of the computation.
- The local computations are performed on a mesh which only depends on the geometry of the body. If B is a collection of identical subdomains, then the local operators are the same, and do not depend on the locations of the holes. Therefore the corresponding matrix has to be stored only once, and "off-line" precomputations (e.g., Cholesky factorization) can be performed outside the fixed point loop. Furthermore, those local computations are fully independent, and therefore they can be performed on different processors.

- Although a proper convergence analysis of the space discretization has still to be done, numerical experiments exhibit good results even when the diameter of the holes are only a few times larger than the global mesh step size.
- This problem can be applied with no modification to interior problems, i.e., to solve Poisson equation in a domain B when the shape of B prevents the use of fast solvers. In this situation we can embed B in a larger domain Ω, simple shaped (e.g., a cube of $\mathbb{R}^N$), where fast solvers can be used.

REFERENCES

1. Dautray, R., and Lions, J. L. (1990). *Mathematical Analysis and Numerical Methods for Science and Technology*, Vol. 1, Springer.
2. Girault, V., and Glowinski, R. (1995). Error analysis of a fictitious domain method applied to a Dirichlet problem. *Japan J. Indust. Appl. Math.* **12**, 487–514.
3. Glowinski, R., and Kuznetsov, Y. (1998). On the solution of the Dirichlet problem for linear elliptic operators by a distributed Lagrange multiplier method. *C. R. Acad. Sci. Paris Sér. I Math.* **327**, 693–698.
4. Glowinski, R., Pan, T.-W., Hesla, T. I., and Joseph, D. D. (1999). A distributed Lagrange Multiplier/fictitious domain method for particulate flows. *Int. J. Multiphase Flow* **25**, 755.
5. McKenney, A., Greengard, L., and Mayo, A. (1995). A fast Poisson solver for complex geometries. *J. Comput. Phys.* **118**, 348–355.
6. Heikkola, E., Kuznetsov, Yu., and Lipnikov, K. (1998). Fictitious domain methods for the numerical solution of 3D acoustic scattering problems. *J. Comp. Acoustics* **7**, 161–183.
7. Heikkola, E., Rossi, T., and Toivanen, J. (2000). *A Parallel Ficitious Domain Method for the Three-Dimensional Helmoltz Equation*, Reports of the Department of Mathematical Information Technology, University of Jyväskylä, Series B. Scientific Computing, No. B9.
8. Le Tallec, P., and Tidriri, M. D. (1999). Convergence analysis of domain decomposition algorithms with full overlapping for the advection-diffusion problem. *Math. Comp.* **68**, 585–606.
9. Leveque, R. J., and Li, Z. (1997). Immersed interface methods for Stokes flow with elastic boundaries or surface tension. *SIAM J. Sci. Comput.* **18**, 709–735.
10. Maury, B. (1999). Direct simulation of 2D fluid particle flows in biperiodic domains. *J. Comput. Phys.* **156**, 325–351.
11. Peskin, C. S., and McQueen, D. M. (1989). A three-dimensional computational method for blood flow in the heart I. Immersed elastic fibers in a viscous incompressible fluid. *J. Comput. Phys.* **81**, 372–405.